Emission mechanism of localized deep levels in BeZnO layers grown by hybrid beam method

J. H. Kim · D. S. Park · J. H. Yu · T. S. Kim · T. S. Jeong · C. J. Youn

Abstract BeZnO layers, which are new materials for ultraviolet-light-emitting devices, were grown by hybrid beam method. The mobility and the carrier concentration on the $Be_xZn_{1-x}O$ layers of $x = 0.28$ were confirmed to be 2.83 cm^2/V s and 4.16×10^{18} cm^{-3}, respectively. Also, the optical properties attributed to the thermal quenching phenomenon of BeZnO were analyzed by photoluminescence as a function of temperature. With increasing temperature, the intensities and the spectral widths on the localized deep-level emissions of 3.6230 eV exponentially reduced and tended to broaden, respectively. Therefore, the temperature dependences of the full width at half maximum and the intensity were explained in terms of a configuration coordinate model. The broad emissions of 3.6230 eV without any fine structure were acted by a strong electron-phonon coupling due to the interaction between the radical beryllium and the ZnO host lattice. In addition, the Frank-Condon shift was found out to be 78.9 meV with the associated phonon energy of 15 meV. Thus, the activation energy of the nonradiative emission participating in the thermal quenching process was estimated to be 48.6 meV. Consequently, its value corresponds to the thermal dissociation energy requiring for the recombination of the conduction electron from the exciting state to the ground state.

Introduction

Ternary alloy materials containing beryllium (Be) have been currently expected as a new candidate for ultraviolet (UV)-light-emitting devices (LED) because of having a large band gap. By changing its Be composition, the band gap can be modulated in the wavelength regions from visible to UV. Owing to such a reason, Be-based ternary compounds have been studied in the II–VI compounds, such as ZnSe or ZnS [1, 2]. BeZnO is one of the materials having an increasing interest too, for the quantum-well structure of BeZnO/ZnO, BeZnO can be utilized as the barrier layer combined with ZnO well. In fact, this structure has been successfully used in UV LED [3]. Despite these results, even tiny pieces of information about the properties of BeZnO are still very limited. Therefore, because of their great potential for technological applications, investigating the optical property of BeZnO is very important. Thus, to find these characterizations, the method of photoluminescence (PL) is usually used. Furthermore, the luminescence mechanism can be well explained by a configuration coordinate (CC) model. This model is based on the assumption of thermal equilibrium including the effect of the nonradiative transitions.

In this work, we grew the BeZnO layers by using a hybrid beam deposition method. Also, we have examined the temperature dependence of PL to clarify the emission mechanisms of BeZnO. Based on the measured PL results, we explained the emission mechanisms of localized deep levels in BeZnO layers through the CC model.

Experimental procedure

BeZnO layers, which were grown on c-Al$_2$O$_3$ substrate, were obtained through the method of hybrid beam

J. H. Kim · D. S. Park · J. H. Yu · T. S. Kim · T. S. Jeong · C. J. Youn (✉)
School of Semiconductor and Chemical Engineering, Chonbuk National University, Jeonju 561-756, South Korea
e-mail: cjyoun@chonbuk.ac.kr

deposition. At this time, the substrate temperature was maintained at 500 °C, and polycrystalline ZnO target was evaporated by an electron beam to create Zn and O sources. At the same time, the Be source was provided from the Be cell by thermal evaporation. The compositional ratio between Be and Zn in the $Be_xZn_{1-x}O$ layers can be controlled by varying the operation temperature of the Be cell. Be has a very low vapor pressure; therefore, the Be effusion cell was operated at a high temperature of 1100 °C. Also, to supply the O elements in the BeZnO layer, the radical O was generated from an oxygen plasma source at the RF power of 300 W. The growth of BeZnO layers was adjusted to the rate of 0.7 Å/s. The thickness of the grown layers was 300 nm. The detailed growth procedures have been published elsewhere [4]. The Be composition and crystal quality in the $Be_xZn_{1-x}O$ were estimated by X-ray diffraction (XRD). The optical properties of the BeZnO layers were investigated by PL. PL measurement was performed at temperatures ranging from 5 to 300 K in a cryostat equipment. The surface of the layer was illuminated by 325-nm UV light emitted from He–Cd laser and the light coming from the sample was dispersed with a monochromator.

Results and discussion

Structural properties

Figure 1 presents the XRD spectra on the BeZnO layers grown under optimized conditions. As shown in Fig. 1, the diffraction peak of BeZnO shifted to a high diffraction angle in comparison to that of ZnO. These patterns correspond to the diffraction peaks of BeZnO(0002) and Al_2O_3(0006). Also, the BeZnO layers are strongly oriented to the c-axis of a hexagonal structure and epitaxially crystallized under constraints created by the substrate. Thus, the lattice constant, C_o, of BeZnO was estimated to be 4.971 Å. According to Vegard's law, the Be rate of x in the grown $Be_xZn_{1-x}O$ layer was calculated to be 0.28. The full width at half maximum (FWHM) of (0002) peak was 0.172°. The mean crystallite size of the film was analyzed using the Scherrer formula [5]:

$$D = 0.94\lambda/(B \cos\theta), \tag{1}$$

where λ, θ, and B are the X-ray wavelength (0.15405 nm), the Bragg diffraction angle, and the FWHM value on (0002) peak in radians, respectively. The mean crystallite size obtained from Eq. 1 was estimated to be about 48 nm. Figure 2 shows the mini-SIMS spectra on the ZnO and BeZnO layers. The existence of the Be component was clearly observed through this experiment. From the XRD and mini-SIMS results, it can be concluded that the Be
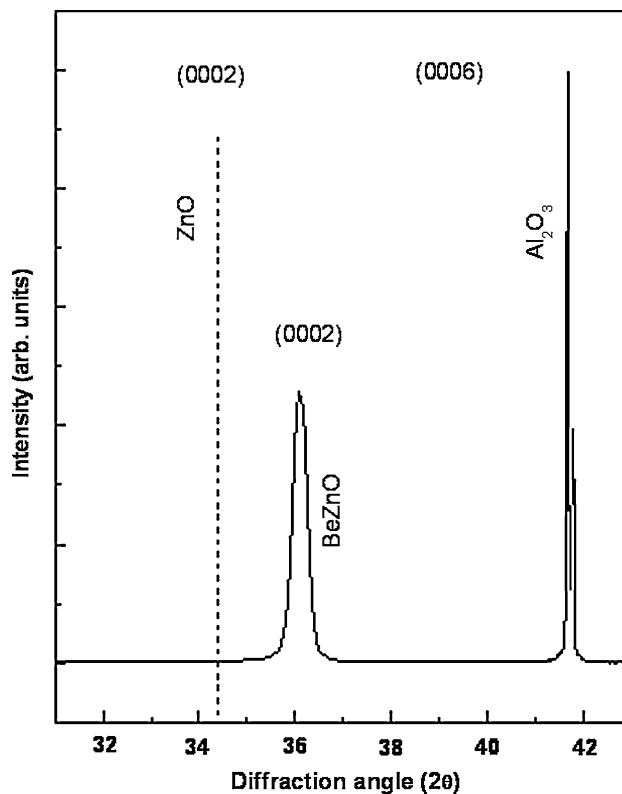
Fig. 1 XRD spectra on the BeZnO layers grown under optimized conditions

component is substituted for the host-lattice site in ZnO. On the other hand, by the Hall effect measurement, the grown BeZnO layers turned out to be an n-type material. Also, the mobility and the carrier concentration on these layers were confirmed to be 2.83 cm²/V s and 4.16×10^{18} cm⁻³, respectively.

Temperature dependence of PL spectra

Figure 3 presents the PL spectra measured at several different temperatures from 5 to 300 K. The broad peaks were observed at the range between 3.75 and 3.3 eV at various temperatures. Thus, these emissions were fixed at the position of 3.6217 eV at a temperature range below 200 K. This phenomenon is related to the increase of alloy disorders caused by the excess injection of Be content. Also, the unique peak of the broad emission can be divided into double peaks using the Gaussian fitting, as shown in the inset of Fig. 3. These divided peaks corresponded to 3.6230 and 3.5476 eV emissions. The 3.6230 eV emissions among the two divided peaks suggested the localized deep-level emissions due to native defects. On the other hand, the $A_l(LO)$ phonons of ZnO and BeO are 576.2 and 1086.2 cm⁻¹, respectively [6, 7]. Therefore, the phonon energy of BeZnO obtained from these compounds was
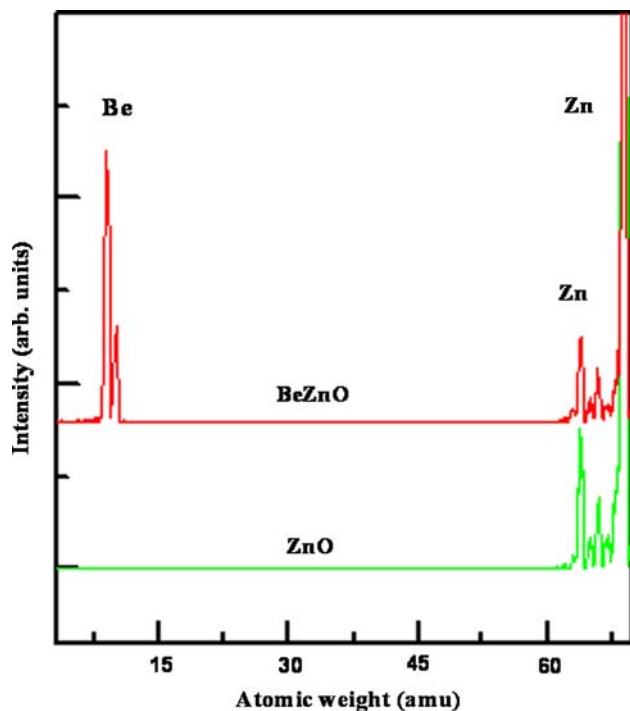
Fig. 2 The mini-SIMS spectrum on the BeZnO layers
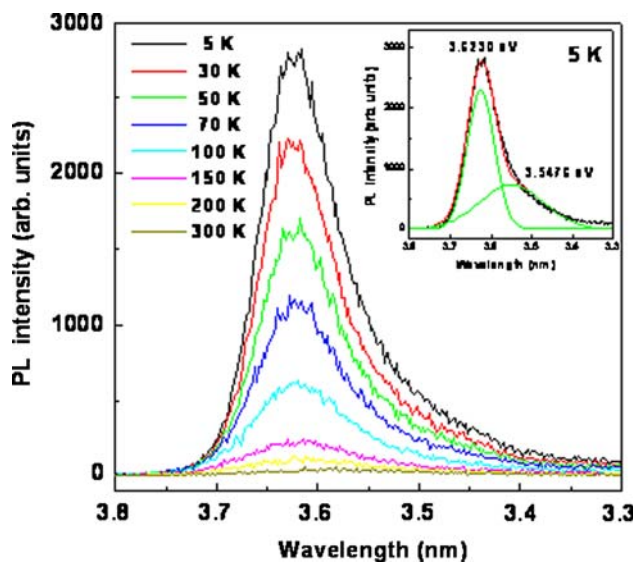
Fig. 3 PL spectra measured at several different temperatures from 5 to 300 K. The inset shows the Gaussian-fitting curves for the spectrum of 5 K

found to be 76 meV according to the linear fitting of compositional rate. Furthermore, the 3.5476 eV emissions are associated with the phonon replica of the 3.6230 eV peak because the energy difference between the two divided emissions is 76 meV. As shown in Fig. 3, the intensities of the PL spectra show the tendency of the increase with decreasing temperature, while the FWHM
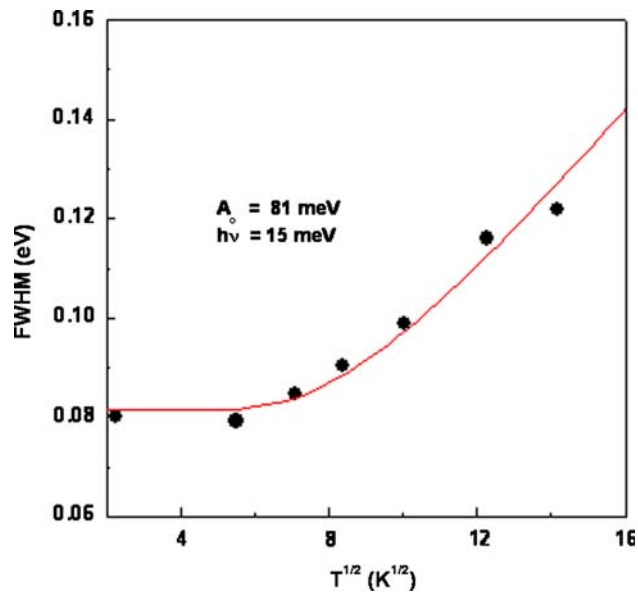
Fig. 4 Temperature dependence of FWHM for the 3.6230 eV emissions

values tend to decrease at the same condition. Therefore, the CC model is a valuable tool in explaining the mechanism of the localized luminescence center in ZnS [8]. According to this model, the temperature dependence of FWHM (W) of the emission is given by [9]

$$W = A_o[\coth(\hbar\omega/2kT)]^{1/2}, \tag{2}$$

where A_o is a constant and the value of A_o is equal to W as the temperature approaches 0 K, $\hbar\omega$ is the effective phonon energy, and k is the Boltzmann constant. Also, A_o corresponds to $(8S_o\ln2)^{1/2}\hbar\omega$, where S_o is the Haung-Rhys electron-phonon coupling constant. The Frank-Condon shift (ΔFC) is given by $\Delta FC = S_o\hbar\omega$. Figure 4 presents the temperature dependence of FWHM for the 3.6230 eV emissions. As Fig. 4 shows, the FWHM remains almost constant till 30 K and then shows the approach at high temperatures to the $T^{1/2}$ dependence of W. Therefore, the solid line fitted by Eq. 2 gives the parameter values of $A_o = 81$ and $\hbar\omega = 15$ meV. The phonon energy does not suggest as a result obtained by the lattice phonons of the host material, because the obtained value is very small. It relates only to a local mode. Therefore, the values of S_o and ΔFC turned out to be 5.26 and 78.9 meV, respectively. But, at deep levels in GaAs, with Haung-Rhys factor $S_o > 5$, a strong electron-lattice coupling is known to exist [10]. It suggests that this phenomenon leads to the 3.6230 eV emission having a broad Gaussian shape without any fine structure. Furthermore, it seems to be related to the high concentration of the radical Be inserted in the ZnO host lattice because the S_o value of the layers with the low rate of Be on the BeZnO composition was smaller than that of

this specimen [11]. Consequently, the Huang–Rhys model should be effectively used to explain the electron-phonon coupling due to the interaction between the radical Be and the ZnO host lattice.

Figure 5 shows the variation of PL intensities with temperatures for the 3.6230 eV emissions. The PL intensity drastically decreased with increasing temperature due to thermal quenching. This is mainly related to thermally activated nonradiative recombination. This luminescence quenching is characterized by relatively high activation energy. The temperature-dependent PL intensity cannot be closely fitted using an Arrhenius plot with a single thermal activation energy but can be well described by the following dual activation energy. This can be derived from the equation [12]:

$$I = I_o/[1 + C_1 \exp(-\varepsilon_1/kT) + C_2 \exp(-\varepsilon_2/kT)], \qquad (3)$$

where C_1 and C_2 are the fitting parameters meaning the relative ratios of nonradiative recombination and ε_1 and ε_2 are the activation energies. Therefore the values calculated from Eq. 3 agree well with the experimental data, as shown in Fig. 5. The activation energies of ε_1 at the intermediate temperature range and ε_2 at the high temperature range are estimated to be 8.3 and 48.6 meV, respectively. The former activation energy is the value corresponding to the binding energy of the deep-level emissions, while the latter activation energy corresponds to the thermal dissociation energy required for the recombination of the conduction electron from the excited state to the ground state.
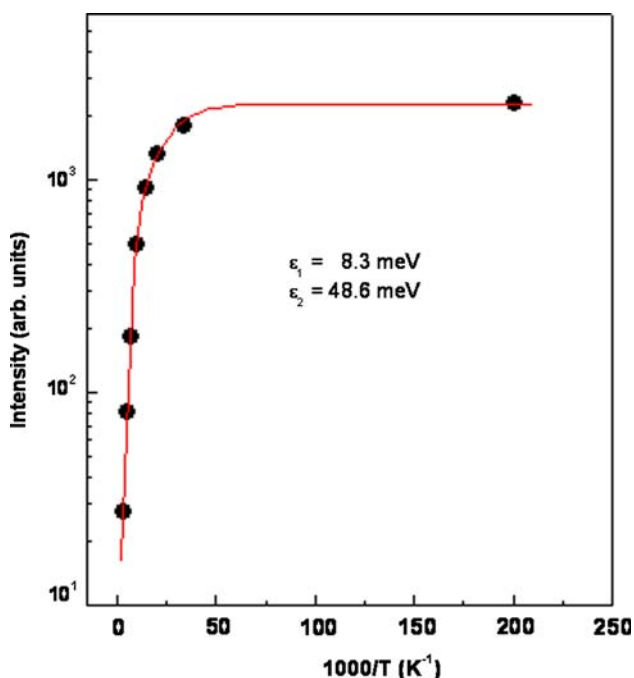
Configuration coordinate diagram

Figure 6 shows the CC diagram of the summarized 3.6230 eV emission. If the ΔFC and the activation energy (ΔE) are present by the CC model, they are equal to those in Fig. 6. When the electron is in the ground state of a minimum potential, the position of the emission center surely locates to Q = 0 point of the average CC. Simultaneously, the potential energy of the ground state is given by a function of $1/2\ k_gQ^2$. Here, k_g is the force constant at the ground state with the vibrational mode. According to the CC model, the electron existed in the ground state of A position and is transited to the excited state of B position due to the energy absorbed from the excitation photon of 325 nm (3.8149 eV). Successively, the electron located to B position transits at the D position via the relaxation process. The potential of the excited state is given as a function of $U + 1/2k_e(Q-Q_o)^2$, where U and k_e are the energy and the force constant at the excited state, respectively. Then, the electron located at the D position is transited to the E position of the ground state. The 3.6230 eV emissions are the result of the recombination between D and E positions. Therefore, the more the transiting electron numbers increase, the more the emission intensity increases. However, this emission usually occurs with lower energies than the energy absorbed from the excitation photon. So, the difference between the absorption and emission maximum is called a Stokes shift and this value is extracted to be 0.1919 eV. Thus, both the

Fig. 5 The variation of PL intensities with temperatures for the 3.6230 eV emissions
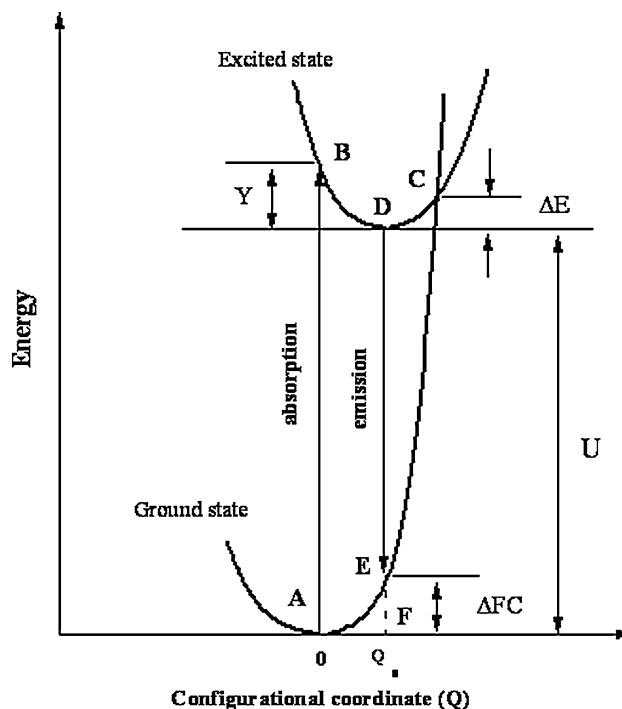
Fig. 6 The CC diagram on the summarized 3.6230 eV emissions

absorption from A to B and emission from D to E require atomic displacements; this is usually shown to be phonon emission, due to the thermal relaxation process. This atomic displacement corresponds to the phonon energy of 15 meV obtained by Eq. 2. Furthermore, when the temperature increases to a high direction, the moved electrons according to the potential curve of the excited state can easily arrive at the C position because of having a fluctuation larger than that at a low temperature. Successively, these electrons arrive at the A position according to potential curve of the ground state. The nonradiative emission is due to the recombination of the electrons participating in this process. Therefore, the more the electron numbers participating in this process, the more the emission intensity is decreased and it should be eventually quenched. As shown in Fig. 5, the PL intensities can be shown to decrease with the increasing temperature. The ΔE, which makes the intensity to be the thermal quenching, is the energy difference between D and C positions at the excited state. Therefore, the ΔE value obtained by Eq. 3 was confirmed to be 48.6 meV at the high temperature region. On the other hand, the ΔFC defined by the difference energy of between E and F positions at the ground state was found to be 78.9 meV as stated above.

Conclusion

BeZnO layers, which are new capable materials for ultraviolet-light-emitting devices, were grown by a hybrid beam method. From the XRD and mini-SIMS results, the Be rate of x in the grown $Be_xZn_{1-x}O$ layer turned out to be 0.28 and it was confirmed that the Be content is substituted for the host-lattice site in ZnO. The optical properties attributed to the thermal quenching phenomenon of BeZnO were studied by PL as a function of temperature. Thus the deep-level emissions and their replica due to native defects were extracted from the localized emissions and divided by the Gaussian fitting. With increasing temperature, the intensities and the spectral widths of the 3.6230 eV emissions exponentially reduced and tended to broaden, respectively. Therefore, the temperature dependences of the FWHM and

the intensity of 3.623 emissions were analyzed in terms of the CC model to explain the recombination mechanism. The S_o value was larger than that of 5 indicating the existence of a strong electron-phonon coupling caused by the interaction between the radical Be and the ZnO host lattice. Therefore, the broad emissions of 3.6230 eV without any fine structure are due to this phenomenon. And the ΔFC was calculated to be 78.9 meV with the associated phonon energy of 15 meV. Thus, with increasing the temperature, the activation energy of the nonradiative emissions participating in the thermal quenching process was estimated to be 48.6 meV. Consequently, it means thermal dissociation energy is required for the recombination of the conduction electron from the excited state to the ground state.

References

1. Maruyama T, Nakamura N, Watanabe M (2002) Jpn J Appl Phys 41:L876
2. Onodera C, Shoji T, Hiratate Y, Taguchi T (2006) Jpn J Appl Phys 45:5821
3. Ryu YR, Lee TS, Lubguban JA, White HW, Kim BJ, Park YS, Youn CJ (2006) Appl Phys Lett 88:241108
4. Han MS, Kim JH, Jeong TS, Park JM, Youn CJ, Leem JH, Ryu YR (2007) J Cryst Growth 303:506
5. Cullity BD (1978) Elements of X-ray diffractions. Addition-Wesley, p 102
6. Youn CJ, Jeong TS, Han MS, Kim JH (2004) J Cryst Growth 261:526
7. Morell G, Perez W, Ching-Prado E, Katiyar RS (1996) Phys Rev B 53:5388
8. Koda T, Shionoya S, Ichikawa M, Minomura S (1966) J Phys Chem Solids 27:1577
9. Klick CC, Schulman JH (1957) In: Seita F, Turnbull D (eds) Luminescence in solids, in solid state physics, vol. 5. Academic, New York, pp 97–172
10. Yu PW (1990) Phys Rev B 42:11889
11. Jeong TS, Kim JH, Youn CJ, submitted to J Cryst Growth
12. Tanaka T, Hayashida K, Nishio M, Guo Q, Ogawa H (2003) J Appl Phys 93:5302